Cryogenic temperatures promote the pressure-induced polymorphic transition in CoCrFeMnNi high entropy alloy

Journal of Applied Physics ARTICLE pubs.aip.org/aip/jap

Cryogenic temperatures promote the pressure-induced polymorphic transition in CoCrFeMnNi high entropy alloy

Cite as: J. Appl. Phys. **136**, 115101 (2024); doi: 10.1063/5.0220107
Submitted: 22 May 2024 · Accepted: 2 September 2024 ·
Published Online: 17 September 2024

Magnus Hörnqvist Colliander,[1,a)] Dörthe Haase,[2] Konstantin Glazyrin,[3] Aina Edgren,[1] Pan Wang,[4] Malcolm Guthrie,[5] and Sheng Guo[6]

AFFILIATIONS

[1]Department of Physics, Chalmers University of Technology, 41296 Gothenburg, Sweden
[2]MAX IV Laboratory, 22484 Lund, Sweden
[3]Deutsches Elektronen-Synchrotron DESY, Notkestr. 85, 22607 Hamburg, Germany
[4]Singapore Institute of Manufacturing Technology (SIMTech), Agency for Science, Technology and Research (A*STAR), Singapore 138634, Singapore
[5]Oak Ridge National Laboratory, Oak Ridge, Tennessee 37830, USA
[6]Department of Industrial and Materials Science, Chalmers University of Technology, 41296 Gothenburg, Sweden

[a)]**Author to whom correspondence should be addressed:** magnus.colliander@chalmers.se

ABSTRACT

Pressure-induced polymorphism has recently been demonstrated in several high entropy alloys. This offers a new window into the much-debated issue of phase selection and stability in these systems. Here, we examine the effect of cryogenic temperatures on the pressure-induced transition from face centered cubic to hexagonal close-packed structures of the prototype CoCrFeMnNi (Cantor) alloy. We observe a reduction in the critical pressure for the onset of the polymorphic transition as the temperature decreases, confirming the progressive stabilization of the hexagonal phase with decreasing temperature previously predicted by *ab initio* calculations accounting for magnetic interactions. We argue that *in situ* high-pressure experiments at cryogenic temperatures, which suppress time-dependent transformation triggered at higher temperatures, present a unique opportunity to significantly improve our understanding of these complex alloys.

I. INTRODUCTION

Following the initial reports,[1,2] so-called high entropy alloys (HEAs), alternatively referred to as multi-principal element alloys (MPEAs) or compositionally complex alloys (CCAs), have received extensive attention due to attractive combinations of properties.[3–11] This class of metallic materials is based on an alternative alloying approach with several (typically in the order of five) elements in approximately equal concentrations, thus defying the traditional "single-element-based alloy" concept. They typically exhibit single- or multi-phase microstructures comprised of face centered cubic (fcc) or body centered cubic (bcc) solid solutions, with rather limited presence of intermetallic phases expected in such systems from an energetic perspective considering the compositional complexity. Hexagonal close-packed (hcp) HEAs do exist[12–15] but are much less common than fcc or bcc, and are often based on rare-earth elements. While the surprising stability of the high-symmetry solid solution phases was initially mainly attributed to the stabilizing effects of the high configurational entropy, many studies have shown that the situation is much more complicated, and there are numerous questions remaining in order to understand the principles of phase selection and thermodynamic/mechanical stability in these systems. Such an understanding is critical for design of alloys relying on deformation-induced phase transformation for strength-ductility trade-off,[6] as well as tailoring of the phase compositions for functional properties.[16]

In this study, we investigate the relative stability of the fcc and hcp phases in the archetypal CoCrFeMnNi (Cantor) alloy[2] using

high-pressure synchrotron x-ray diffraction (HPXRD) experiments performed at cryogenic temperatures. In spite of the fact that it is one of the first discovered and most widely studied HEAs, the phase selection is not yet fully understood. The current understanding, derived mainly from *ab initio* calculations,[17–20] indicates that fcc is stabilized relative to hcp by magnetic moment contributions, where both magnetic entropy[17] and frustration[19] have been proposed as the responsible mechanisms. Calculations predict that hcp should be stabilized relative to fcc with decreasing temperature, and even become the stable phase at sufficiently low temperatures.[17] At high temperatures, on the other hand, fcc becomes increasingly stable, and the alloy thus solidifies in this polymorph when cooled from the molten state.

However, experimentally probing the relative stability as a function of temperature is difficult. At intermediate temperatures precipitation of secondary phases[21–24] will change the chemistry and free energy landscape, while the increasing energy penalty associated with hcp phase formation is too large to allow the transformation to be provoked. At low temperatures, the kinetics of any spontaneous phase transformation will be too slow to measure under realistic time scales, even for situation where thermodynamics dictates that it must occur at equilibrium. The latter could be the reason why no temperature-driven fcc-to-hcp transition has been observed at cryogenic temperatures,[25] even if the predicted stability of hcp would be correct.

Recently, CoCrFeMnNi has been shown to undergo a sluggish polymorphic transition from fcc to hcp during hydrostatic compression (where only limited dislocation activity is expected) at room temperature.[26–29] Interestingly, a comparison with ternary and quarternary derivatives shows that while CoCrFeNi behaved similar to the quinary Cantor alloy, ternary CoCrNi exhibited only limited formation of the hcp phase.

In CoCrFeMnNi, the transition starts at pressures in the range of 8–20 GPa (strongly affected by stress hydrostaticity and microstructural state[28]) and hcp volume fractions close to 100% are reached at pressures around 40–50 GPa. The fraction of deformation-induced twin boundaries in CoCrFeMnNi deformed under non-hydrostatic (typically uniaxial) conditions, on the other hand, remains low even at very large strains at cryogenic temperatures.[30] This indicates that the almost complete transformation of fcc to hcp during hydrostatic compression is *not* plasticity-induced, but rather an effect of changes in the relative thermodynamic stability of the phases, or removal of kinetic barriers. This allows controlled application of hydrostatic pressure to be used as a tool for probing the phase stability. In particular, by performing high-pressure experiments at varying cryogenic temperatures, we can study the temperature effects on the pressure-induced transition without the limitations of slow thermal activation kinetics at low temperatures or phase-separation effects at higher temperatures.

Here, we report the results of HPXRD experiments performed at temperatures down to 30 K. We demonstrate that this approach can be used to study the relative stability of fcc and hcp phases in CoCrFeMnNi through the temperature-dependence of the pressure-induced polymorphic transition. We show that a decreasing temperature promotes the transition from fcc to hcp, which suggests a relative stabilization of hcp with decreasing temperature in agreement with previous predictions from *ab initio* calculations.[17] We also point out future directions for high-pressure experiments in order to further investigate the underlying physical mechanism.

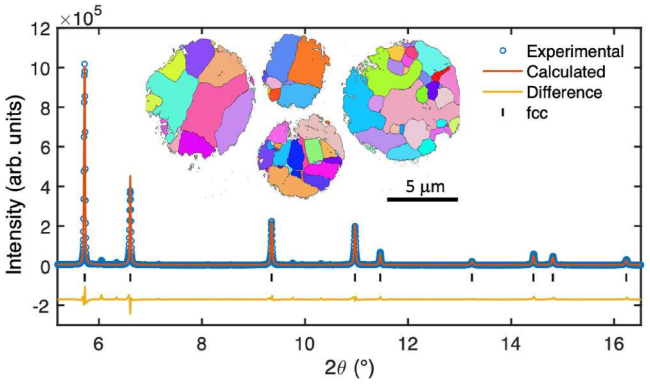

FIG. 1. Diffractogram from the CoCrFeMnNi powder obtained under ambient condition (room temperature, ambient pressure), including results of the Pawley fitting. The presence of minor impurity peaks is marked with black diamonds. The inset shows EBSD maps of several particles, confirming the polycrystalline microstructure.

II. EXPERIMENTS

Equiatomic CoCrFeMnNi was obtained in the form of a powder with an average particle size of 10.3 ± 6.1 μm, produced using vacuum induction melting gas-atomization with argon gas.[31] The size of individual grains in the particles were in the range of 1–5 μm, as indicated by the electron backscatter diffraction (EBSD) maps of four individual particles in Fig. 1 (inset). The EBSD maps were collected using a LEO Gemini 1550 SEM (Carl Zeiss, Germany) operated at 30 keV, equipped with a Nordlys EBSD detector (Oxford Instruments, UK) and analyzed using MTEX software.[32]

Ambient pressure powder diffraction was performed at the P02.1 Powder Diffraction and Total Scattering Beamline at PETRA III, DESY, Germany,[33] using a photon energy of 59.90 keV [wavelength λ = 0.2073 Å and a downstream VAREX XRD 4343CT area detector at a distance of approximately 2 m (the exact detector position was calibrated with data obtained from a NIST 660C LaB_6 standard)]. The CoCrFeMnNi powder was contained in 1 mm borosilicate capillaries. The recorded detector images were reduced to 1D diffractograms using PyFAI v.0.21.3.[34,35] Figure 1 shows the resulting 1D diffractogram and the corresponding Pawley fitting for extraction of the lattice parameter. The powder showed a single-phase fcc structure, although with very minor presence of unidentified impurity phases and a lattice parameter of $a = 3.592\,54(3)$ Å.

The HPXRD experiments were performed at the P02.2 Extreme Conditions Beamline at PETRA III, DESY, Germany.[36] Powder particles were compressed in membrane-loaded diamond anvil cells (DACs) in an axial geometry with Ne as the pressure transmitting medium (PTM). We used a culet size of 300 μm, together with Re gaskets which were pre-compressed to 40 μm thickness. Laser drilling was used to make a 100 μm hole in the gasket, in which the sample was loaded together with gold and ruby particles as pressure markers. Ruby fluorescence was used to approximately control the pressure during ramps, while the equation of state (EoS) of gold[37] was used to determine the actual

pressures from the (111) peak position. The beam size was $3 \times 8\,\mu m^2$ and the photon energy was 42.69 keV ($\lambda = 0.2904$ Å). Diffraction patterns corresponding to gold and sample were collected at pressures up to around 55 GPa using a Perkin Elmer XRD 1621 area detector placed 0.372 m behind the sample position (calibrated with a CeO_2 standard). For cryogenic measurements, three different DAC assemblies were cooled to the target temperature (180, 100, or 30 K) in a He flow-cryostat before application of pressure. Each detector image was azimuthally integrated using Dioptas v.0.5.7[38] (using masks to remove strong reflections from the diamond anvils when present) to produce 1D diffractograms for further analysis.

III. RESULTS

A. Data quality and analysis

No signs of the hcp phase could be observed in the as-loaded states, confirming the absence of a purely temperature-induced transition. Gradual disappearance of fcc peaks and appearance of hcp peaks occurred at all temperatures, indicating occurrence of the expected polymorphic transition. Due to the small beam size relative to the powder particles, the diffraction patterns do not correspond to ideal powder average, see Figs. 2(a) and 2(b) for examples of detector images recorded at 2.2 GPa (initial pressure) and 51.3 GPa (final pressure) at room temperature. Futhermore, Ne crystallizes at ~4.8 GPa at room temperatures and significantly earlier at lower temperatures,[39] resulting in the appearance of strong Bragg peaks in the diffractograms. Masking the Ne peaks was generally avoided, as the Ne peaks traverse a wide 2θ range, overlapping with both fcc and hcp peaks [see Fig. 2(c)]. Accidental masking of fcc and hcp peaks when attempting to mask Ne peaks could therefore significantly affect the evaluation of phase fractions.

Evaluation of the diffractograms can be done either by fitting of selected individual diffraction peaks for each phase, or by whole-pattern refinement (Rietveld method) or fitting (Pawley/LeBail methods). We explored all three approaches (single-peak fitting, Rietveld refinement, and Pawley fitting) using GSAS-II,[40] with an instrument parameter file obtained from the CeO_2 data. A thorough description of the different methods and a comparison of the resulting cell volumes (V) and hcp phase fractions (f_{hcp}) are provided in the supplementary material. In conclusion, Rietveld refinements were found to be significantly more stable than Pawley fitting and consequently have been used to determine cell volumes. We have critically examined the utility of refinements for our heavily textured data sets, and demonstrated its suitability as described in the supplementary material. Example of refinements results for the initial and final pressures at room temperature are shown in Figs. 2(d) and 2(e). Single-peak fitting was used to extract the hcp phase fractions, as Rietveld refinement was unable to accurately capture the early stages of the transformation. Error bars for phase fractions were obtained from measurements of several sample positions at constant pressure during the room temperature test.

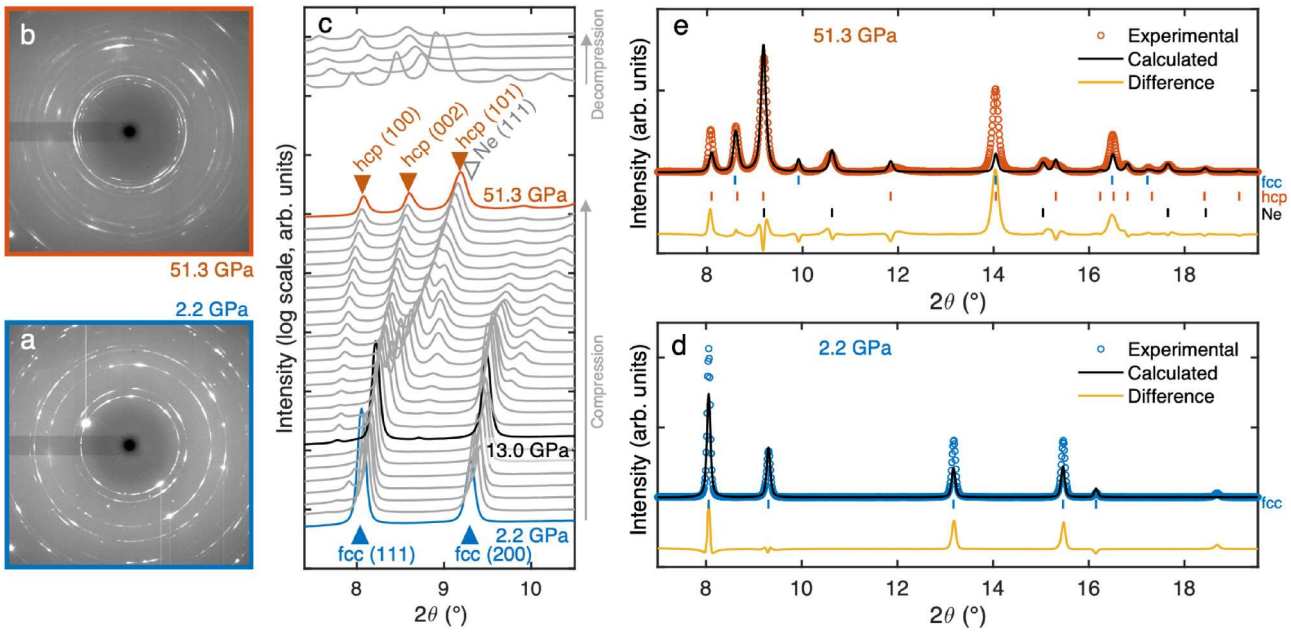

FIG. 2. Compression of CoCrMnFeNi powder at room temperature. (a) and (b) show detector images recorded at room temperature in the initial state (2.2 GPa) and at the maximum pressure (51.3 GPa), respectively. Note the strong reflections from the diamond present in the initial state, which were always masked during reduction when present. (c) Series of 1D diffractograms, off-set vertically for clarity. The black line (13.0 GPa) corresponds to the pressure where both (100) and (101) peaks of the hcp phase were clearly visible. (d) and (e) Results of Rietveld refinements of the 1D diffractograms obtained at 2.2 and 51.3 GPa.

B. Room temperature behavior

Before a more detailed analysis of the data from the experiments at cryogenic temperatures, we first confirm the agreement between our room temperature data and previous studies. Figure 2(c) shows the gradual transition from fcc to hcp with increasing pressure. The diffractogram shown in black indicates the pressure where the presence of both (100) and (101) peaks of the hcp phase could be clearly observed. This is shown in more detail in Fig. 3(a), which focuses on the region around the fcc (111) peak where the hcp peaks are observed, for the diffractograms recorded at pressures around the transition. As mentioned, the critical pressure for the onset of the phase transition was not well captured by the Rietveld refinements. Instead, thorough manual inspection of the 1D diffractograms was used to identify the presence of hcp [defined as unambiguous observation of both the (100) and (101) peaks of the hcp phase]. The critical pressure for onset of the transformation (p^*) is reported as the average of the pressure where the presence of hcp phase was identified, and the next lower pressure (error bars correspond to half the difference between the two pressures). According to this definition, the resulting value of p^* at room temperature is 12.5 $\pm$ 0.5 GPa, within the typical (broad) range of previously reported onset pressures.[26–29] The onset pressure is slightly below the tentative quasi-hydrostatic limit for Ne (around 15 GPa[41,42]) which should delay the transition,[29] whereas the relatively large grain size of the gas-atomized powder should decrease the critical pressure.[29] The observed value, which is in the middle of the range of previously reported pressures for onset of the transformation, is therefore reasonable. Similar to previous reports, the transition is sluggish, occurring over the pressure range of 15–50 GPa, see Fig. 3(b). Also, the saturation fraction is consistent with earlier studies, around 0.9, and is reached at similar pressures.

The retention of the hcp phase has been a point of discussion in previous studies. Zhang *et al.*[27] reported almost no change in the hcp fraction after decompression, whereas Tracy *et al.*[26] found that 60% of the hcp phase formed during compression was retained after decompression, independent of the pressure from which the material was decompressed. We measured the hcp fraction after fully releasing the pressure in the membrane (which yielded a partial decompression to 33 GPa), and at a number of lower pressures obtained by manually releasing the tightening screws in a stepwise manner. We observe a constant hcp fraction down to around 5 GPa, after which a partial reversion occurs. At 0 GPa, we measure an hcp fraction of approximately 0.7 (78% of the saturation fraction). It is likely that the reversion of the transformation during decompression behavior is strongly sample-dependent and may potentially be related to grain size, particle size and compression/decompression rate and hydrostaticity in a manner similar to the transition during compression. Nevertheless, the partial reversion of the high-pressure phase upon decompression suggests that the hcp phase is *not* thermodynamically stable at room temperature, contrary to predictions from *ab initio* calculations.[17] The fact that the hcp fraction appears to be constant down to pressures around 5 GPa, below which the reversion occurs, clearly points to the need for further dedicated studies to understand the stabilizing effect of pressure on the hcp phase and its reversion, including the associated kinetics and temperature dependence.

Figures 4(a) and 4(b) show the pressure-dependent cell volumes for fcc and hcp, respectively, which agree very well with the results of Tracy *et al.*[26] and Zhang *et al.*[27] The pressure-dependence of the cell volume was fitted with a third order Birch–Murnaghan equation of state (EoS),[43,44]

$$p = \frac{3B_0}{2}\left[\left(\frac{V}{V_0}\right)^{\frac{7}{3}} - \left(\frac{V}{V_0}\right)^{\frac{5}{3}}\right]\left\{1 + \frac{3}{4}\left(B_0' - 4\right)\left[\left(\frac{V}{V_0}\right)^{\frac{2}{3}}\right]\right\}, \quad (1)$$

where V_0 is the reference volume (at ambient pressure), B_0 is the bulk modulus, and B_0' is the pressure derivative of B_0. The EosFit-7 software[45,46] was used to perform the fitting, and the results are shown in Table I. For the fcc phase V_0 was constrained to the value obtained from the separate room temperature diffraction experiments (see Sec. II), which is assumed to be the most accurate value. The value of B_0 for the fcc phase is smaller than those reported by Tracy *et al.*[26] and Zhang *et al.*,[27] but our value [142(2) GPa] is in very good agreement with experimental reports from dedicated tests of the elastic properties of CoCrFeMnNi at room temperature (144 GPa,[3] 140 GPa,[47] 137 GPa,[48] and 143 GPa[49]). Our value of B_0' for the fcc phase is slightly higher than previous reports but still in reasonable agreement.

As no separate ambient-pressure measurement of the hcp volume was performed, Eq. (1) was fitted without constraints. As

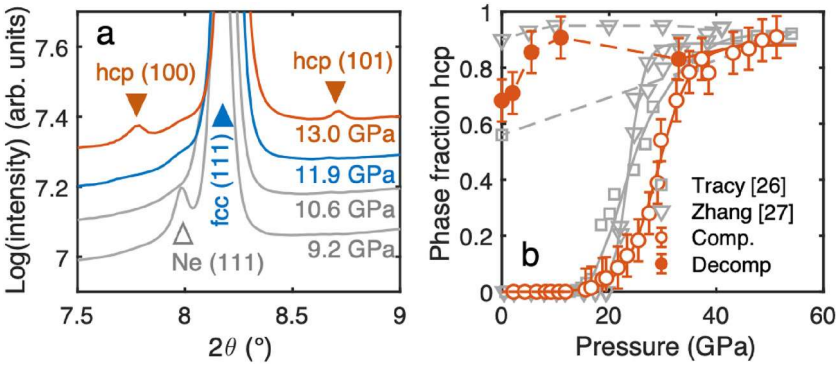

FIG. 3. (a) Magnification of the region around the fcc (111) peak where the hcp (100) and (101) peaks are located, showing their absence at 11.9 GPa and presence at 13.0 GPa (black line). (b) Evolution of the hcp phase fraction with pressure during both compression (denoted "Comp.," shown with open symbols) and decompression (denoted "Decomp.," shown with closed symbols) at room temperature, compared with the results from Tracy *et al.*[26] and Zhang *et al.*[27]

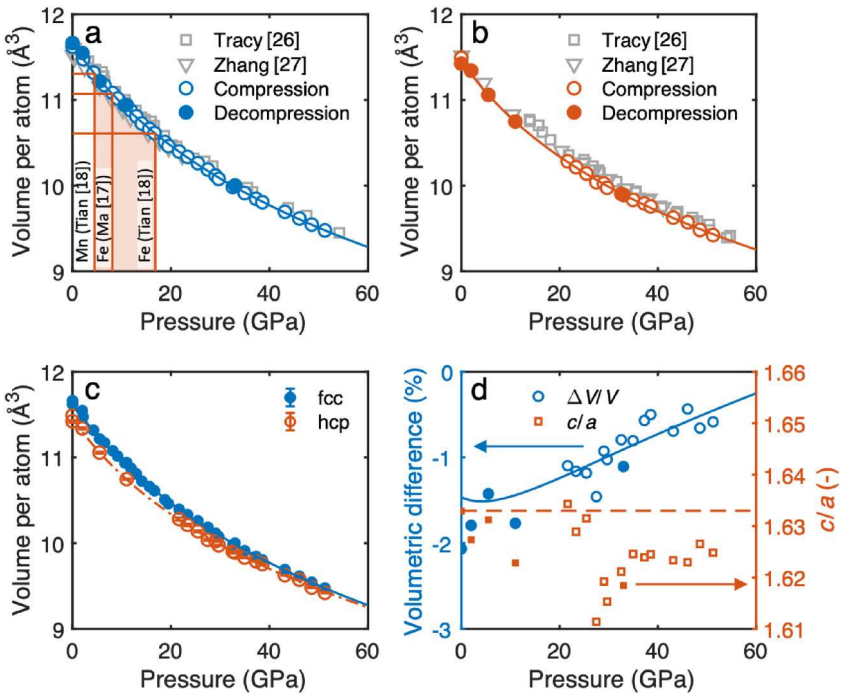

FIG. 4. Cell volume of (a) fcc and (b) hcp phases with applied pressure, fitted with third order Birch–Murnaghan EoS, as described in the text, compared with data from Tracy *et al.*[26] and Zhang *et al.*[27] Open symbols correspond to data collected during compression, and closed symbols correspond to decompression. The red lines in (a) show predicted pressures where the magnetic moments of Fe[17,18] and Mn[18] vanish, and the corresponding volume per atom. (c) Comparison of the pressure-dependent cell volume of both phases. (d) Evolution of the volumetric difference between the hcp and fcc phase ($\Delta V/V = (V_{fcc}/V_{hcp} - 1) \times 100$), and the c/a ratio for the hcp phase. Open symbols correspond to data from compression, closed symbols denotes data from decompression. The solid blue line shows V_{fcc}/V calculated from the fitted EoS for the two phases, and the dashed red line indicates the ideal c/a from a hard-sphere model (1.633).

for the fcc phase, our value of B_0 for the hcp phase is somewhat lower than previous reports, whereas B_0' is slightly higher. However, relatively small changes in the value of V_0 will affect the resulting values of B_0 and B_0' quite drastically, and as the values of V_0 were not reported by Tracy *et al.*[26] and Zhang *et al.*,[27] it is difficult to pinpoint the reasons for the differences between the studies.

Comparing the pressure-dependent cell volumes of the two phases [Figs. 4(c) and 4(d)], we confirm the small volume collapse associated with the fcc-to-hcp transition reported by Tracy *et al.*,[26] and in good agreement with the theoretically predicted value of 0.9% at 0 K.[17] We also note that the c/a ratio of the hcp phase, 1.625(6), is slightly lower than the ideal value of 1.633, in good agreement with Tracy *et al.*,[26] indicating a preferential contraction of the unit cell along the c direction. No significant trend in terms of pressure-dependence could be observed for the c/a ratio.

C. Effect of cryogenic temperatures

After confirming that we can reproduce the previously reported results within reasonable margins, we proceed to investigate the effect of cryogenic temperatures on the pressure-induced phase transition. Figure 5(a) compares the gradual transition from fcc to hcp with increasing pressure at all temperatures. The onset of the transition occurs at lower pressures at cryogenic temperatures compared to room temperature, while the saturation fractions are similar. We note a slight change in the behavior of the sample tested at 100 K, occurring around 25 GPa. This is a result of light shift of the sample with respect to the beam at this pressure, causing a new set of grains fulfilling Bragg conditions. Anisotropic elastic interactions in the polycrystalline powder particles will cause differences in hydrostaticity between different crystals, and hence the new set of diffracting crystals would have undergone a slightly different pathway. Nevertheless, the final phase fractions at the highest pressures are very similar to the tests at higher and lower temperatures. The measured pressures at the transformation onset, p^*, are 6.8(11) GPa at 30 K, 7.6(4) GPa at 100 K, and 9.1(4) GPa at 180 K, compared to 12.5(5) GPa at 300 K as reported above. Figure 5(b) shows the temperature-dependence of p^*, where the decrease is well described by a second order polynomial expression. However, we point out that the error bar (representing the difference between the lowest pressure where unambiguous hcp peaks could be observed, and the next lower pressure) is large for the sample tested at 30 K due to the relatively large step between the two subsequent pressure levels (5.7 and 7.8 GPa). The difference between the onset pressure at 100 K [7.6(4)] and 30 K [6.8(11)] can therefore not be considered statistically significant.

Unfortunately, the phase stability upon reversion could not be investigated at cryogenic temperatures, as the DACs would have to be heated to room temperature and removed from the cryostat to enable manual compression beyond the residual pressure after full release of the membrane pressure. Rietveld refinement of the data collected after full release of the membrane pressure (corresponding to a pressure of around 30 GPa) resulted in hcp fraction similar to those at maximum pressure, which is expected given that the hcp phase was stable down to 5 GPa at room temperature. Consequently, we are not able to draw conclusions regarding the effect of temperature on the relative stability of the phases during decompression.

TABLE I. Comparison of zero-pressure reference volume (V_0), the bulk modulus (B_0), and its pressure derivative (B_0') from a third order Birch–Murnaghan EoS fit with literature values.

	fcc			hcp		
	V_0 (Å^3)	B_0 (GPa)	B_0' (–)	V_0 (Å^3)	B_0 (GPa)	B_0' (–)
Zhang *et al.*[27]	…	154(3)	4.9(7)	…	150(5)	6.2(5)
Tracy *et al.*[26]	…	150(3)	5.1(4)	…	141(8)	5.6(2)
This study	11.63	142(2)	5.5(2)	11.46(3)	137(8)	6.9(5)

To examine the kinetics of the transition at different temperatures, we fitted the data at each temperature using the logistic equation

$$f_{\mathrm{hcp}}(p) = \frac{f_\infty}{1 + \exp[-\eta(p - p_0)]}, \tag{2}$$

where f_∞, η, and p_0 are fitting parameters. The resulting midpoint slope, given by $m = \eta f_\infty/4$, is shown as a function of temperature in Fig. 5(b). The midpoint slope appears to decrease slightly with decreasing temperature, although the effect is relatively weak, and even for $\alpha = 0.1$ the confidence interval for a linear fit is relatively large. Fitting a second order polynomial only slightly improves the fit, but significantly increases the confidence interval. While the observed trend suggests a temperature-dependent kinetics of the transformation, the uncertainty is too large to support any firm conclusions without further dedicated experiments. Here, we also note that the slightly different behavior of the 100 K sample in the range of 30–45 GPa (after the previously described sample shift) leads to an underestimation of f_∞, in spite of the actual phase fraction at saturation for the 100 K sample being similar to the other temperatures.

The pressure-dependent cell volumes for both the fcc and hcp phases are shown in Fig. 6 for all temperatures. The effect of temperature is very small for both phases, as can be seen from Figs. 7(a) and 7(b). This is expected, as the temperature only has a minor effect on V_0 (based on the temperature-dependent lattice parameter measurements by Schneeweiss *et al.*[25] the volume decrease upon cooling to 30 K is only 0.9%) and B_0 (being only a few GPa higher at 30 K compared to room temperature[3,49]). Consequently, any effect of temperature on the EoS is too small to be reliably determined beyond the uncertainty in the refinements.

As seen in Fig. 6, the cell volume of the hcp phase is smaller than fcc at all temperatures, and the volumetric difference between the fcc and hcp phases does not show any systematic dependence on temperature or pressure, see Fig. 7(c). The value of the volume collapse based on data from all temperatures is 0.74(47)%. Similarly, the unit cell distortion of the hcp phase (preferential c axis contraction) appears to be unaffected by temperature, see Fig. 7(d). While Tracy *et al.*[26] reported a continuous decrease in the c/a ratio with increasing pressure, the scatter is too large in our data to draw firm conclusions. Considering the data from all temperatures, we find an average c/a ratio of 1.619(12).

In summary, while there is a pronounced effect of decreasing temperature on the onset pressure for the polymorphic transition, the effects on the relative size of the fcc and hcp unit cells, the distortion of hcp cell, and the pressure-dependence of the cells (EoS) appear to be negligible.

IV. DISCUSSION

The decreasing critical pressure with decreasing temperature is in general agreement with the predicted increasing stability of the hcp phase with decreasing temperature.[17] As mentioned, both magnetic entropy[17] and magnetic frustration[19] have been proposed as the origin of fcc stability. Magnetic frustration arises as the combination of antiferromagnetic Cr and Mn with ferromagnetic Co, Fe,

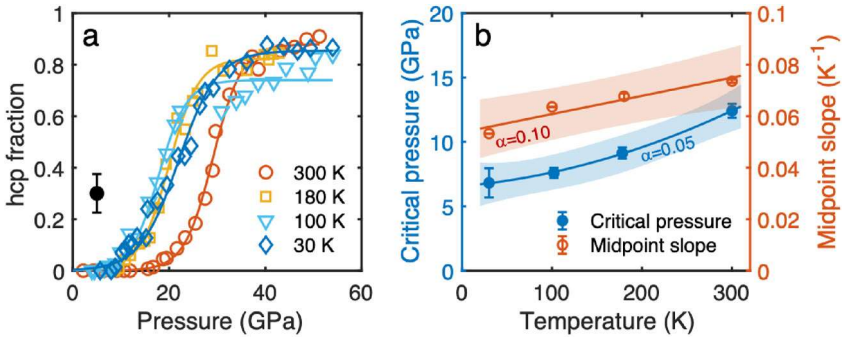

FIG. 5. (a) Evolution of the hcp phase fraction with pressure at all tested temperatures. The solid lines are fits of Eq. (2) to each data set. The black marker with error bars shows the typical uncertainty. (b) Temperature-dependence of the critical pressure p^* and the midpoint slope m from the fits of Eq. (2). The solid lines are polynomial fits to the data (second and third order, respectively, for the critical pressure and midpoint slope), and shaded regions show the corresponding 95% ($\alpha = 0.05$, critical pressure) or 95% ($\alpha = 0.10$, midpoint slope) confidence intervals.

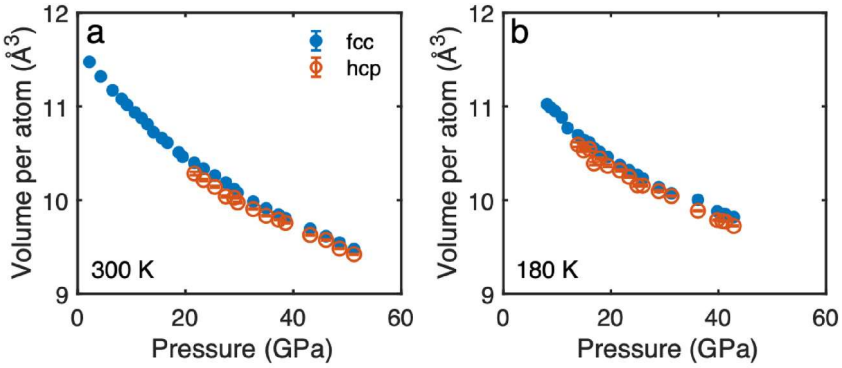

FIG. 6. Cell volumes for the fcc and hcp phases during compression at different temperatures. (a) 300 K; (b) 180 K; (c) 100 K; and (d) 30 K.

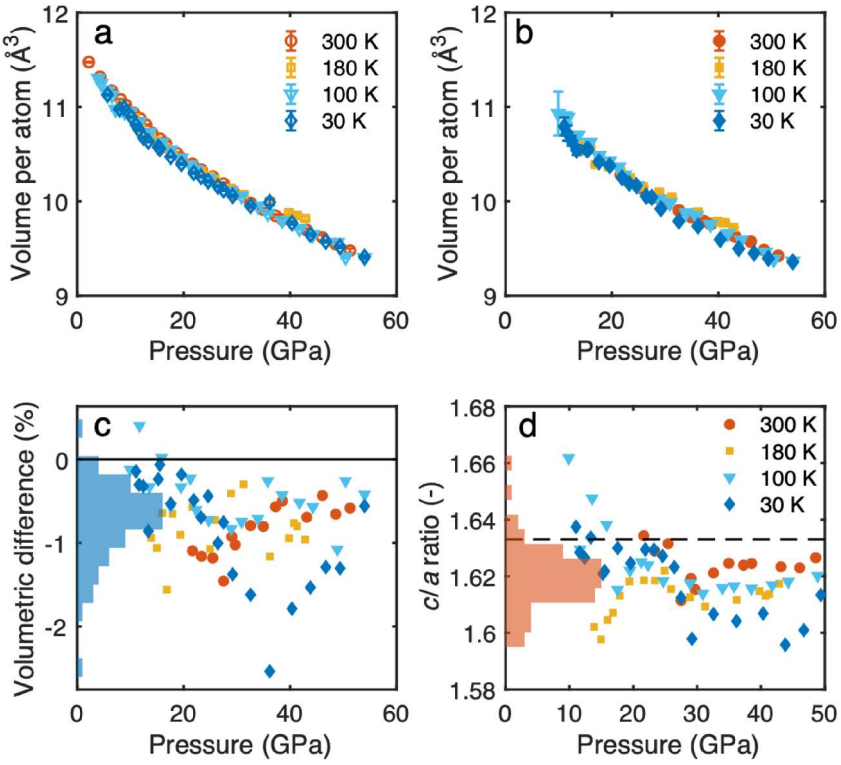

FIG. 7. Pressure-dependent cell volume for (a) fcc and (b) hcp at all tested temperatures (data from compression only). (c) and (d) show the volumetric difference between the two phases and the c/a ratio of the hcp phase, respectively, as a function of pressure. The histograms on the left axes in (c) and (d) is based on the data from all temperatures. The dashed horizontal line in (d) indicates the ideal c/a ratio for hcp calculated from a hard sphere model (1.633).

and Ni does not allow preferred magnetic moment alignments to be completely satisfied.[19] Common for the two mechanisms is that they rely on the presence of non-zero atomic magnetic moments. Ni is generally accepted to be non-magnetic in CoCrFeMnNi, and the magnetic moments of Co and Cr are significantly smaller than for Mn and Fe.[17–19] The non-zero moments are predicted to decrease when the volume is decreased, and at some point vanish.[17,18] Pressure-induced suppression of magnetic moments have been experimentally measured in e.g., pure Co, Fe, and Ni[50] and $Ni_{1-x}Mn_x$.[51]

Ma *et al.*[17] predicted the only (significant) magnetic moment in CoCrFeMnNi to belong to Fe, and the complete suppression of this at a volumetric strain of −5%. Returning to the measured atomic volumes in Fig. 4(a), this corresponds to a volume around 11.1 $Å^3$, and consequently a pressure of around 9 GPa. The soft-core calculations by Tian *et al.*,[18] on the other hand, suggest that both Fe and Mn have non-zero magnetic moments at ambient pressure, and that these are suppressed at volumetric strains of −3% (Mn) and −9% (Fe). These volumetric strains correspond to atomic volumes of 11.3 $Å^3$ (Mn) and 10.6 $Å^3$ (Fe), or pressures of 5 GPa (Mn) and 18 GPa (Fe) according to Fig. 4(a). While the uncertainties in the values are large, they nevertheless coincide with the experimentally determined pressure range for the polymorphic transition onset, thereby supporting the proposed magnetic moment-induced stabilization of fcc and the gradual destabilization by pressure-induced magnetic moment suppression.

We note that this could be further explored using x-ray emission spectroscopy (XES) or x-ray magnetic circular dichroism (XMCD), which are able to resolve the magnetic moments of individual atomic species. In the case of Fe, also synchrotron Mössbauer spectroscopy presents an alternative method. As these techniques are compatible with high-pressure experiments using DACs, the element-specific pressure-induced magnetic moment suppression should be experimentally accessible. Ideally, experiments where such measurements are combined with simultaneous collection of diffraction data could be used to directly correlate magnetic moment evolution with the onset of the structural transformation. Such studies would certainly shed further light on the correlation between magnetic moments and the phase stability, and, in particular, should be able to differentiate between the roles of Fe and Mn. In particular, as the magnetic frustration model for the fcc stabilization depends on the contribution by Mn, detailed knowledge of the pressure-dependent magnetic moment of Mn is of specific interest.

In this context, we must also note that there is ample experimental evidence of magnetic transitions in CoCrFeMnNi at cryogenic temperatures. The alloy is paramagnetic at room temperature, but several studies have measured two transitions during cooling, the first occurring at 93 K[25] or 85 K[52,53] and the second at 38 K[25] or 43 K.[52,53] There is, at present, no general agreement as to the nature of the transitions. While Schneeweiss *et al.*[25] and Elmslie *et al.*[53] suggest that the first transition (at 85–93 K) is a result of spin-freezing to form a spin-glass state, Kamarád *et al.*[52] proposed ferrimagnetic ordering. The second transition (at 38–43 K) has been attributed to spin-freezing[52] as well as ferromagnetic[25] and ferrimagentic[53] ordering. One study found only a single transition, at 20 K, which was attributed to spin-freezing.[54]

While the details are unclear, the presence of magnetic transition(s) could certainly be expected to affect the pressure-induced phase transition. The three highest temperatures in this study (100, 180, and 300 K) are all above the first magnetic transition (85–93 K), and the alloy can be assumed to be paramagnetic. This is the state predicted by *ab initio* calculations, and the effects and correlations predicted by the previously cited studies should therefore be valid. Detailed studies of the temperature dependence in the range of 30–100 K, where magnetic transitions occur, could provide further insights into the correlations between the magnetic state and the phase stability.

As a final note, we return to the previously mentioned dependence on both microstructure and hydrostaticity on the onset of the polymorphic transition.[28] While the microstructure can be considered to be constant in the present case, as random particles from the same batch was used for all runs, the deviations from hydrostatic conditions can be expected to change with temperature. The crystallization of Ne will occur at lower pressures as the temperature is decreased,[39] which will lower the quasi-hydrostatic limit. However, as the onset of the transition occurs below the quasi-hydrostatic limit, as determined from the room temperature run for which the limit is known,[41,42] we expect the effect to be relatively small, and primarily affect the observed kinetics rather than the onset pressure. A comparative study of the temperature-dependence of the onset pressure in different PTMs would shed further light on the contribution from reduced hydrostaticity.

V. CONCLUSION

In summary, we have shown that cryogenic high-pressure diffraction offers the possibility to investigate phase stability and selection in HEA systems by combining variable pressure and temperature but avoiding the complications associated with structural decomposition at higher temperatures. Specifically, we have shown that the onset pressure for the polymorphic fcc-to-hcp transition in CoCrFeMnNi decreases with decreasing temperature, while the effects on the unit cells and their pressure-dependence are small.

We propose that a thorough investigation of the temperature range where magnetic transitions occur is of outmost importance for a deeper understanding. Furthermore, we suggest that diffraction experiments should be combined with *in situ* high-pressure spectroscopy measurements, such as XES and XMCD, which can resolve element-specific magnetic moments and thereby provide insights into the underlying mechanisms.

SUPPLEMENTARY MATERIAL

See the supplementary material for a description and comparison of different methods for determining cell volumes and phase fractions (single-peak fitting, Rietveld refinement, whole-pattern Palwey fitting), and a motivation for the approaches chosen.

ACKNOWLEDGMENTS

We acknowledge DESY (Hamburg, Germany), a member of the Helmholtz Association HGF, for the provision of experimental facilities. Parts of this research were carried out at beamlines P02.1

and P02.2 at PETRA III, where beamtime was allocated for Proposal Nos. I-20210528 EC and I-20230084 EC. M.G. was supported by resources at the Spallation Neutron Source and the High Flux Isotope Reactor, Department of Energy (DOE) Office of Science User Facilities operated by the Oak Ridge National Laboratory. Bala Malladi acknowledges for the EBSD analysis.

AUTHOR DECLARATIONS

Conflict of Interest

The authors have no conflicts to disclose.

Author Contributions

Magnus Hörnqvist Colliander: Conceptualization (lead); Data curation (lead); Formal analysis (lead); Investigation (equal); Methodology (equal); Visualization (lead); Writing – original draft (lead); Writing – review & editing (lead). **Dörthe Haase:** Investigation (equal); Methodology (equal); Writing – review & editing (supporting). **Konstantin Glazyrin:** Investigation (supporting); Methodology (supporting); Writing – review & editing (supporting). **Aina Edgren:** Investigation (equal); Writing – review & editing (supporting). **Pan Wang:** Resources (supporting); Writing – review & editing (supporting). **Malcolm Guthrie:** Conceptualization (equal); Methodology (equal); Writing – review & editing (supporting). **Sheng Guo:** Investigation (equal); Writing – review & editing (supporting).

DATA AVAILABILITY

The data that support the findings of this study are available from the corresponding author upon reasonable request.

REFERENCES

[1]J. W. Yeh, S. K. Chen, S. J. Lin, J. Y. Gan, T. S. Chin, T. T. Shun, C. H. Tsau, and S. Y. Chang, Adv. Eng. Mater. **6**, 299–303 (2004).
[2]B. Cantor, I. T. Chang, P. Knight, and A. J. Vincent, Mater. Sci. Eng. A **375–377**, 213–218 (2004).
[3]B. Gludovatz, A. Hohenwarter, D. Catoor, E. H. Chang, E. P. George, and R. O. Ritchie, Science **345**, 1153–1158 (2014).
[4]Y. Zou, H. Ma, and R. Spolenak, Nat. Commun. **6**, 7748 (2015).
[5]Z. J. Zhang, M. M. Mao, J. Wang, B. Gludovatz, Z. Zhang, S. X. Mao, E. P. George, Q. Yu, and R. O. Ritchie, Nat. Commun. **6**, 2–7 (2015).
[6]Z. Li, K. G. Pradeep, Y. Deng, D. Raabe, and C. C. Tasan, Nature **534**, 227–230 (2016).
[7]Z. Lei, X. Liu, Y. Wu, H. Wang, S. Jiang, S. Wang, X. Hui, Y. Wu, B. Gault, P. Kontis, D. Raabe, L. Gu, Q. Zhang, H. Chen, H. Wang, J. Liu, K. An, Q. Zeng, T. G. Nieh, and Z. Lu, Nature **563**, 546–550 (2018).
[8]Z. Li, S. Zhao, R. O. Ritchie, and M. A. Meyers, Progr. Mater. Sci. **102**, 296–345 (2019).
[9]Q. Ding, Y. Zhang, X. Chen, X. Fu, D. Chen, S. Chen, L. Gu, F. Wei, H. Bei, Y. Gao, M. Wen, J. Li, Z. Zhang, T. Zhu, R. O. Ritchie, and Q. Yu, Nature **574**, 223–227 (2019).
[10]E. P. George, D. Raabe, and R. O. Ritchie, Nat. Rev. Mater. **4**, 515–534 (2019).
[11]M. Cagirici, P. Wang, F. L. Ng, M. L. S. Nai, J. Ding, and J. Wei, J. Mater. Sci. Technol. **94**, 53–66 (2021).
[12]M. C. Gao, B. Zhang, S. M. Guo, J. W. Qiao, and J. A. Hawk, Metall. Mater. Trans. A **47**, 3322–3332 (2016).
[13]J. W. Qiao, M. L. Bao, Y. J. Zhao, H. J. Yang, Y. C. Wu, Y. Zhang, J. A. Hawk, and M. C. Gao, J. Appl. Phys. **124**, 195101 (2018).
[14]B. Akhil, A. Bajpai, N. P. Gurao, and K. Biswas, Modell. Simul. Mater. Sci. Eng. **29**, 085005 (2021).
[15]A. Ter-Isahakyan, J. S. Rau, and T. J. Balk, J. Alloys Compd. **893**, 162293 (2022).
[16]K. Biswas, N. P. Gurao, T. Maiti, and R. S. Mishra, *High Entropy Materials* (Springer Nature, Singapore, 2022), pp. 259–287.
[17]D. Ma, B. Grabowski, F. Körmann, J. Neugebauer, and D. Raabe, Acta Mater. **100**, 90–97 (2015).
[18]F. Tian, L. K. Varga, J. Shen, and L. Vitos, Comput. Mater. Sci. **111**, 350–358 (2016).
[19]C. Niu, C. R. LaRosa, J. Miao, M. J. Mills, and M. Ghazisaeidi, Nat. Commun. **9**, 1–9 (2018).
[20]J. Šebesta, K. Carva, and D. Legut, Phys. Rev. Mater. **3**, 124410 (2019).
[21]M. Laurent-Brocq, A. Akhatova, L. Perrière, S. Chebini, X. Sauvage, E. Leroy, and Y. Champion, Acta Mater. **88**, 355–365 (2015).
[22]F. Otto, A. Dlouhý, K. G. Pradeep, M. Kuběnová, D. Raabe, G. Eggeler, and E. P. George, Acta Mater. **112**, 40–52 (2016).
[23]E. J. Pickering, R. Muñoz-Moreno, H. J. Stone, and N. G. Jones, Scr. Mater. **113**, 106–109 (2016).
[24]N. D. Stepanov, D. G. Shaysultanov, M. S. Ozerov, S. V. Zherebtsov, and G. A. Salishchev, Mater. Lett. **185**, 1–4 (2016).
[25]O. Schneeweiss, M. Friák, M. Dudová, D. Holec, M. Šob, D. Kriegner, V. Holý, P. Beran, E. P. George, J. Neugebauer, and A. Dlouhý, Phys. Rev. B **96**, 014437 (2017).
[26]C. L. Tracy, S. Park, D. R. Rittman, S. J. Zinkle, H. Bei, M. Lang, R. C. Ewing, and W. L. Mao, Nat. Commun. **8**, 1–6 (2017).
[27]F. Zhang, Y. Wu, H. Lou, Z. Zeng, V. B. Prakapenka, E. Greenberg, Y. Ren, J. Yan, J. S. Okasinski, X. Liu, Y. Liu, Q. Zeng, and Z. Lu, Nat. Commun. **8**, 15687 (2017).
[28]F. Zhang, H. Lou, S. Chen, X. Chen, Z. Zeng, J. Yan, W. Zhao, Y. Wu, Z. Lu, and Q. Zeng, J. Appl. Phys. **124**, 115901 (2018).
[29]E. W. Huang, C. M. Lin, J. Jain, S. R. Shieh, C. P. Wang, Y. C. Chuang, Y. F. Liao, D. Z. Zhang, T. Huang, T. N. Lam, W. Woo, and S. Y. Lee, Mater. Today Commun. **14**, 10–14 (2018).
[30]W. Fu, W. Zheng, Y. Huang, F. Guo, S. Jiang, P. Xue, Y. Ren, H. Fan, Z. Ning, and J. Sun, Mater. Sci. Eng. A **789**, 139579 (2020).
[31]P. Wang, P. Huang, F. L. Ng, W. J. Sin, S. Lu, M. L. S. Nai, Z. L. Dong, and J. Wei, Mater. Des. **168**, 107576 (2019).
[32]F. Bachmann, R. Hielscher, and H. Schaeben, "Texture Analysis with MTEX – Free and Open Source Software Toolbox," Solid State Phenomena **160**, 63–68 (2010).
[33]A. C. Dippel, H. P. Liermann, J. T. Delitz, P. Walter, H. Schulte-Schrepping, O. H. Seeck, and H. Franz, J. Synchrotron Radiat. **22**, 675–687 (2015).
[34]G. Ashiotis, A. Deschildre, Z. Nawaz, J. P. Wright, D. Karkoulis, F. E. Picca, and J. Kieffer, J. Appl. Crystallogr. **48**, 510–519 (2015).
[35]J. Kieffer, V. Valls, N. Blanc, and C. Hennig, J. Synchrotron Radiat. **27**, 558–566 (2020).
[36]H. P. Liermann, Z. Konôpková, W. Morgenroth, K. Glazyrin, J. Bednarčik, E. E. McBride, S. Petitgirard, J. T. Delitz, M. Wendt, Y. Bican, A. Ehnes, I. Schwark, A. Rothkirch, M. Tischer, J. Heuer, H. Schulte-Schrepping, T. Kracht, and H. Franz, J. Synchrotron Radiat. **22**, 908–924 (2015).
[37]P. I. Dorogokupets and A. Dewaele, High Pressure Res. **27**, 431–446 (2007).
[38]C. Prescher and V. B. Prakapenka, High Pressure Res. **35**, 223–230 (2015).
[39]W. L. Vos, J. A. Schouten, D. A. Young, and M. Ross, J. Chem. Phys. **94**, 3835–3838 (1991).
[40]B. H. Toby and R. B. Von Dreele, J. Appl. Crystallogr. **46**, 544–549 (2013).
[41]S. Klotz, J.-C. Chervin, P. Munsch, and G. Le Marchand, J. Phys. D **42**, 075413 (2009).
[42]K. Takemura, High Pressure Res. **41**, 155–174 (2021).
[43]F. D. Murnaghan, Proc. Natl. Acad. Sci. U.S.A. **30**, 244–247 (1944).
[44]F. Birch, Phys. Rev. **71**, 809–824 (1947).
[45]R. J. Angel, J. Gonzalez-Platas, and M. Alvaro, Z. Kristallogr. **229**, 405–419 (2014).

[46]J. Gonzalez-Platas, M. Alvaro, F. Nestola, and R. Angel, J. Appl. Crystallogr. **49**, 1377–1382 (2016).
[47]Z. Wu, H. Bei, G. M. Pharr, and E. P. George, Acta Mater. **81**, 428–441 (2014).
[48]G. Laplanche, P. Gadaud, O. Horst, F. Otto, G. Eggeler, and E. P. George, J. Alloys Compd. **623**, 348–353 (2015).
[49]A. Haglund, M. Koehler, D. Catoor, E. P. George, and V. Keppens, Intermetallics **58**, 62–64 (2015).
[50]V. Iota, J. H. P. Klepeis, C. S. Yoo, J. Lang, D. Haskel, and G. Srajer, Appl. Phys. Lett. **90**, 1–4 (2007).
[51]J. Kamarád, J. Kudrnovský, Z. Arnold, V. Drchal, and I. Turek, High Pressure Res. **31**, 116–120 (2011).
[52]J. Kamarád, M. Friák, J. Kaštil, O. Schneeweiss, M. Šob, and A. Dlouhý, J. Magn. Magn. Mater. **487**, 165333 (2019).
[53]T. A. Elmslie, J. Startt, S. Soto-Medina, Y. Yang, K. Feng, R. E. Baumbach, E. Zappala, G. D. Morris, B. A. Frandsen, M. W. Meisel, M. V. Manuel, R. Dingreville, and J. J. Hamlin, Phys. Rev. B **106**, 014418 (2022).
[54]P. Koželj, S. Vrtnik, M. Krnel, A. Jelen, D. Gačnik, M. Wencka, Z. Jagličić, A. Meden, F. Danoix, J. Ledieu, M. Feuerbacher, and J. Dolinšek, J. Magn. Magn. Mater. **523**, 1–10 (2021).